J. Marine. Sci. Appl. (2012) 11: 169-177
DOI: 10.1007/s11804-012-1119-0

Pilot Study on the Oscillation and Migration of a Spherical Bubble Escaping from the Lateral Propulsion Hole

Baoyu Ni[1,2*], Shaoshi Dai[1], Rui Han[1], Longquan Sun[1] and Hailong Chen[1]

1. College of Shipbuilding Engineering, Harbin Engineering University, Harbin 150001, China
2. Department of Mechanical Engineering, University College London, Torrington Place, London WC1E 7JE, UK

Abstract: In an atrocious ocean environment, the lateral propulsion hole could potentially be partly out of water and capture an air cavity. Bubbles would form when the captured air cavity escapes underwater and they may affect the performance of the sonar. The common commercial computational fluid dynamics software CFX was adopted to calculate the ambient flow field around the lateral propulsion hole generated by a moving vessel. The oscillation of the spherical bubble was based on the Rayleigh-Plesset equation and its migration was modeled using the momentum equation. The radiated noise of the oscillating bubble was also studied. The aim is that the results from this paper would provide some insight into corresponding fluid and acoustic study.
Keywords: Lateral propulsion hole; bubble oscillation; migration; radiated noise
Article ID: 1671-9433(2012)02-0169-09

1 Introduction

Under an atrocious ocean environment, the lateral propulsion hole could potentially be partly out of water and capture an air cavity. When the lateral propulsion hole goes underwater as the vessel heaves, the air captured would escape from the lateral propulsion hole because of buoyancy. There are two main forms of air that could escape: one is masses of air with the length scale in the order of half the diameter of the lateral propulsion hole; the other is small bubbles with the length scale in the order of one percent diameter of the lateral propulsion hole. With combined effects of ocean currents, waves, and buoyancy, the escaped bubbles would move upwards as well as abaft. Apart from the migration, the bubbles would also oscillate in high frequency and radiate noise. In this way, the migration and oscillation of bubbles may influence the performance of the ship's sonar. A better understanding of the migration and radiated noise of bubbles escaping from the lateral propulsion hole would be very useful to improve the sonar's effectiveness, which has important engineering significance.

There is a large body of research literature on how bubbles rise underwater. In the review of bubble dynamics, Prosperetti (2004) mentioned that bubbles would rise in the water in three stages: straight, zig-zag, and spiral. Vries *et al.* (2002) studied the path and wake of gas bubbles rising at high Reynolds numbers in highly purified water with an experiment. They first found that zig-zagging bubbles had a double-threaded wake and the wake was unstable some distance downstream of the bubble. Wang and Tong (2008) numerically simulated the deformation and motion of a bubble rising in a narrow vertical tube using the Level Set Method and Volume of Fluid Method, and the numerical results agreed well with the experimental data. Gu *et al.* (2007) modeled the distribution of bubbles in ships' far field wakes with using a RANS equation and bubble transport equation, and studied the bubbles' density distribution, the bubble wake expanding regularity, and the damping law of the bubbles' number; Shi *et al.* (2007) analyzed the migration and oscillation of bubbles in the ships' wake theoretically, and simulated the motion of bubbles in different radii and different gas compositions numerically. Fu *et al.* (2011) adopted a VOF model and mixture multiphase model in the general CFD code FLUENT6.3.26 and introduced different turbulence models to simulate the bubbly wake in the near field after a surface ship.

However, as far as the authors know, to this point there have not been any numerical simulations on the motion of bubbles around the lateral propulsion hole and their radiated noise. To solve this problem, this paper tracks a spherical bubble using a mixed Eulerian/Lagrangian method and studies its oscillation and migration in the ambient flow generated by a moving vessel. The ambient flow is calculated using the Eulerian method, while the trajectory of the bubble is tracked using the Lagrangian method. The one-way coupled particle tracking method (OCPTM) is adopted to obtain the oscillation and migration of the bubble by the simultaneity of a Rayleigh-Plesset equation and Momentum Theorem.

Received date: 2012-03-16
Foundation item: Supported by the National Science Foundation of China (11002038) , Key Project of National Natural Science Funds (50939002), National Defense Foundation Scientific Project (B2420110011), the National Science Foundation for Young Scientists of China (51009035), and Natural Science Funds of Heilongjiang Province (E201047,A200901).
***Corresponding author Email:** baoyuni@gmail.com

2 Bubble dynamic model

After Rayleigh (1917) erected the ideal spherical bubble motion equation (RP Equation), Cole (1948), Gilmore *et al.* (1952), and Plesset and Chapman (1971) modified the equation in different views and got a variety of modified equations considering different effects. Among them, a classical example is seen below, which considers the gas component, viscosity, and surface tension.

$$R\ddot{R}+\frac{3}{2}\dot{R}^2=\frac{1}{\rho}\left[P_c+P_{g0}(\frac{R_0}{R})^{3\gamma}-\frac{2\sigma}{R}-4\mu\frac{\dot{R}}{R}-P_v\right] \quad (1)$$

where R is the bubble radius, ρ is the liquid density, P_c is the saturated vapor pressure, P_{g0} and R_0 are the initial gas pressure and bubble radius, γ is the ratio of the specific heat of the gas, σ is the surface tension, μ is the dynamic viscosity ratio, and P_v is the ambient liquid pressure.

Eq.(1) does not consider the effect of relative slip velocity between the bubble and the carrying liquid. To account for this slip velocity, an additional pressure term $(\boldsymbol{v}-\boldsymbol{u}_b)^2/4$, is added to the classical RP equation as (see Appendix for detailed derivation):

$$R\ddot{R}+\frac{3}{2}\dot{R}^2=\frac{1}{\rho}\left[P_c+P_{g0}(\frac{R_0}{R})^{3\gamma}-\frac{2\sigma}{R}-4\mu\frac{\dot{R}}{R}-P_v\right]+\frac{(\boldsymbol{v}-\boldsymbol{u}_b)^2}{4} \quad (2)$$

where $\boldsymbol{u}_b$ is the travel velocity of the bubble center, which is a function of time. $\boldsymbol{v}$ is the ambient flow velocity.

The oscillation of the bubble is determined by the RP equation while the trajectory is decided by the force state of the bubble. The differential equation of motion can be obtained as below (Hsiao *et al.*,2000）.

$$\rho_b\frac{4}{3}\pi R^3\frac{\mathrm{d}\boldsymbol{u}_b}{\mathrm{d}t}=\frac{4}{3}\pi R^3(\rho_b-\rho)\boldsymbol{g}-\frac{4}{3}\pi R^3\nabla P_v+\frac{1}{2}\rho\pi R^2C_D(\boldsymbol{v}-\boldsymbol{u}_b)\left|\boldsymbol{v}-\boldsymbol{u}_b\right|+\frac{2}{3}\pi R^3\rho(\frac{\mathrm{d}\boldsymbol{v}}{\mathrm{d}t}-\frac{\mathrm{d}\boldsymbol{u}_b}{\mathrm{d}t})+2\pi R^2\dot{R}\rho(\boldsymbol{v}-\boldsymbol{u}_b)+6\pi R^2\sqrt{\frac{\rho\mu}{\pi}}\int_0^t\frac{\frac{\mathrm{d}\boldsymbol{v}}{\mathrm{d}t}-\frac{\mathrm{d}\boldsymbol{u}_b}{\mathrm{d}t}}{\sqrt{t-\tau}}\mathrm{d}\tau \quad (3)$$

The physical meaning of each item on the right hand of this equation is buoyancy, pressure gradient, drag force, added mass force which contains two items caused by translating and radial oscillating, respectively, and memory effect force (also known as Basset term), where ρ_b is the density of the gas in the bubble.

The bubble drag coefficient C_D can be determined by using the empirical equation of Haberman and Morton (1953),

$$C_D=\frac{24}{R_{eb}}\left(1+0.197R_{eb}^{0.63}+2.6\times10^{-4}R_{eb}^{1.38}\right) \quad (4)$$

where the bubble Reynolds number is defined as $R_{eb}=2\rho R\left|\boldsymbol{v}-\boldsymbol{u}_b\right|/\mu$.

$\mathrm{d}\boldsymbol{v}/\mathrm{d}t$ and pressure gradient ∇P_v have the relationship listed below according to a Navier-Stokes equation.

$$\frac{\mathrm{d}\boldsymbol{v}}{\mathrm{d}t}=\boldsymbol{g}-\frac{\nabla P_v}{\rho}+\frac{\mu\nabla^2\boldsymbol{v}}{\rho} \quad (5)$$

Substitute equation (5) into (3), ignore the Basset term and take $\rho_b\approx\rho/820$ into consideration as well, the simplified bubble motion differential equation is as shown below.

$$\frac{\mathrm{d}\boldsymbol{u}_b}{\mathrm{d}t}=-\boldsymbol{g}-\frac{3}{\rho}\nabla P_v+\frac{3}{4}\frac{C_D}{R}(\boldsymbol{v}-\boldsymbol{u}_b)\left|(\boldsymbol{v}-\boldsymbol{u}_b)\right|+\frac{3}{R}(\boldsymbol{v}-\boldsymbol{u}_b)\dot{R}+\frac{\mu}{\rho}\nabla^2\boldsymbol{v} \quad (6)$$

Equations (2) and (6) are both second-order nonlinear ordinary differential equations, which can be solved with a fourth-order Runge-Kutta scheme by integrating through time. In this paper, the ambient pressure P_v and velocity $\boldsymbol{v}$ are calculated by the common CFD software CFX based on the NS equation. Take the calculated pressure P_v and velocity $\boldsymbol{v}$ as the initial input of the first time step, solve Eq.(2) and (6) simultaneously and obtain the information such as the location, velocity, and radius of the bubble. Input the new information into CFX and get the ambient pressure P_v and velocity $\boldsymbol{v}$ at the new position of the bubble. Then take the new ambient parameters as the input of the next time step and loop until the end condition satisfies (such as the total calculating time obtaining certain value $T_{\text{total}}\geq\tilde{T}$).

The OCPTM model used in this paper is based on several assumptions. First, the bubble size is much smaller than the length scale of the ambient flow and the presence of the bubble can be ignored for the ambient flow. Second, the bubble oscillation period is much smaller than the time scale of the ambient flow. Third, the bubble is so small that the asphericity of bubble surface can be ignored. Fourth, the fluid is incompressible due to low speed of the vessel and the bubble motion. Under these assumptions, the flow chart of this procedure is shown in Fig.1.

After obtaining the information of the bubble's oscillation, the radiated pressure at the distance of l from the center is determined by the equation below (Hsiao and Chahine, 2003):

$$P=\frac{\rho}{l}(R^2\ddot{R}+2R\dot{R}^2)-\rho(\frac{R^4\dot{R}^2}{2l^4}) \quad (7)$$

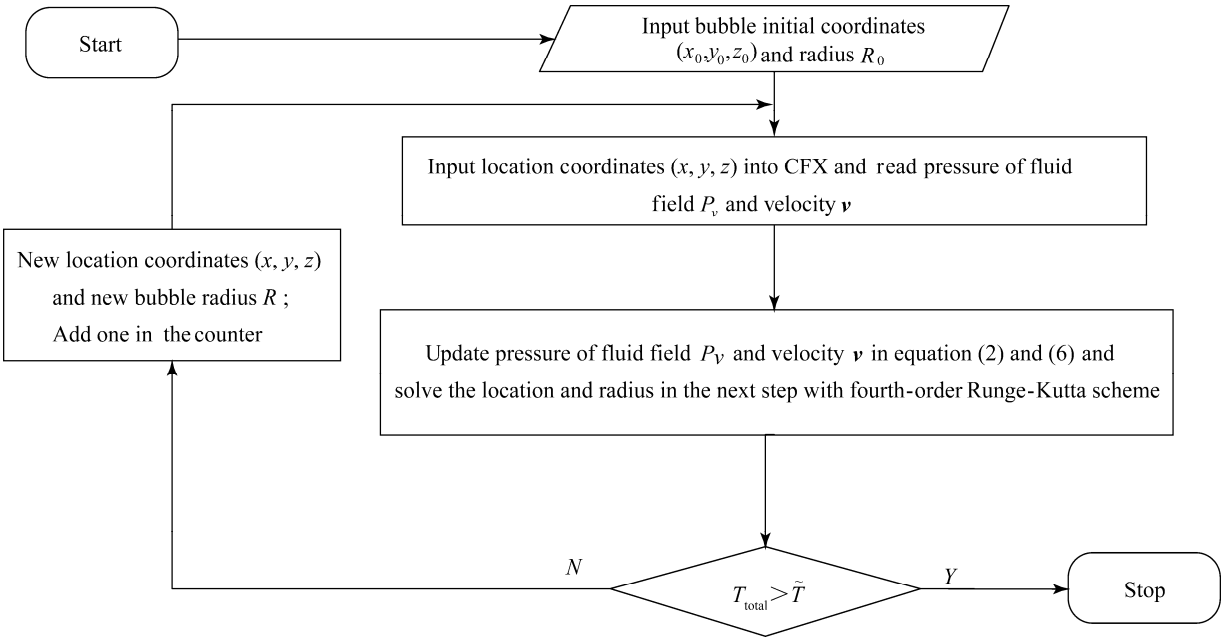

Fig.1 The flow chart of the one-way coupled particle tracking method

When $l >> R$, equation (7) will be transformed into the formulation of radiated acoustic pressure given by Fitzpatrick and Strasberg (1958):

$$P_a(t') = \frac{R\rho}{l}[R\ddot{R}(t') + 2\dot{R}^2(t')], \quad t' = t - \frac{l-R}{c} \tag{8}$$

where t' is the delayed time due to the finite sound speed c.

The sound pressure level (SPL) can be written as follows:

$$\mathrm{SPL} = 20\log(\frac{P_a}{P_{\mathrm{ref}}}) \tag{9}$$

where reference pressure is taken $P_{\mathrm{ref}} = 10^{-6}\ \mathrm{N/m^2}$.

3 Ambient flows calculated with CFX

The common CFD software CFX is adopted to simulate the flow field around a moving vessel with a lateral propulsion hole. This paper uses VOF to capture the free surface, and adopts the SIMPLE method to solve the NS equation, where the convective item is in second-order precision. An SST turbulence model is used to define parameters for the calculated flow in the characteristics of velocity distribution in the infinite water-depth theory. Because of the complicated hull, this paper adopts software ICME to construct topology and uses block O grid-unstructured grid division technology to discretize the flow field. In particular, the grids near the bulbous bow, lateral propulsion hole, and stern are refined to improve numerical accuracy, while grids become sparse in the far field. The Computational Grid in the fluid region is composed of 860 thousand units and 810 thousand nodes. The geometrical model and local magnified image is shown in Fig.2.

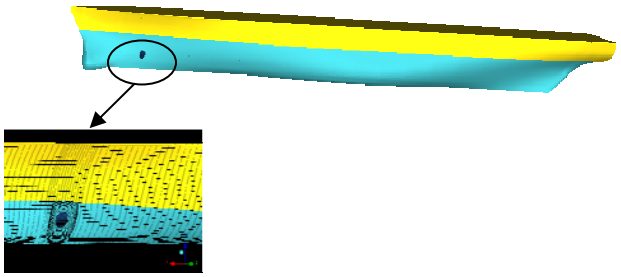

Fig.2 The geometrical model of a trial vessel and the local magnified image of grids near the lateral propulsion hole

Boundary conditions of the fluid field are defined in Table 1, where the inlet velocity is determined by the conditions of infinite water depth.

Table 1 Boundary Conditions of the Flow Field

Boundary of the Flow Field	Boundary Condition in VOF
Top	Opening
Inlet	Velocity of Infinite Water Depth
Outlet	Out Static Pressure
Wall of Ship	No Slip Wall
Other Faces	Free Slip Wall

Initial conditions for the calculation are defined in Table 2, where the wave is taken as a 3rd plane translatory wave.

Table 2 Initial Conditions for the Calculation

Fluid	Reference Pressure/ Pa	1.02×10^5
	Initial Velocity/ ($m\cdot s^{-1}$)	0
	Temperature/℃	15
	Density/ ($kg\cdot m^{-3}$)	1020
Vessel	Initial Velocity/kn	8
	Heaving Amplitude /m	0.94
Wave	Height /m	0.88
	Period /s	7.5

The volume fraction of the fluid and velocity vector on the section of the lateral propulsion hole are calculated by CFX and plotted in Fig.3 and Fig.4, when the vessel heaves to the lowest point.

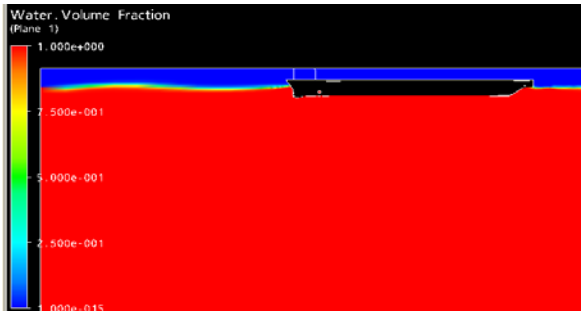

Fig.3 The volume fraction of the fluid

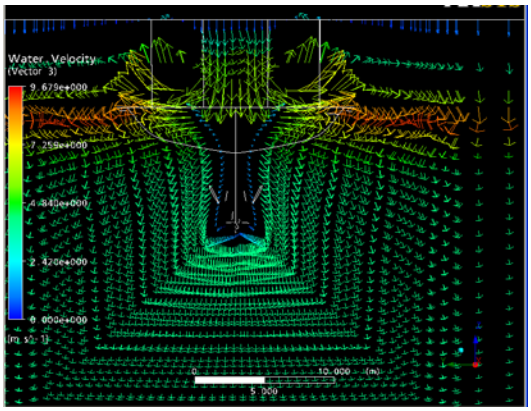

Fig.4 Velocity vector graph on the section of lateral propulsion hole

4 Numerical Simulation of Bubble Dynamic Response

Based on the method mentioned above, dynamic responses of a small spherical bubble under different conditions are studied. Take the initial radius of the bubble as 1/50 and 1/100 of the diameter D_1 of lateral propulsion hole, respectively. Here, assume the initial escaping moment for the bubble to be when the vessel heaves to the lowest point, and the initial escaping position to be the top of the lateral propulsion hole. The influence of the bubble's oscillation is excluded and included in the simulation, respectively, as seen below.

4.1 Without the Influences of Bubble's Oscillation

First, the influence of the bubble's oscillation is not considered. This means ignoring the effects of Eq.(2) and neglecting added mass force $3\dot{R}(\boldsymbol{v}-\boldsymbol{u}_b)/R$ caused by radial oscillation in Eq.(6) during the calculation. In this way, the bubble is actually taken as a sphere with a stable diameter during the calculation.

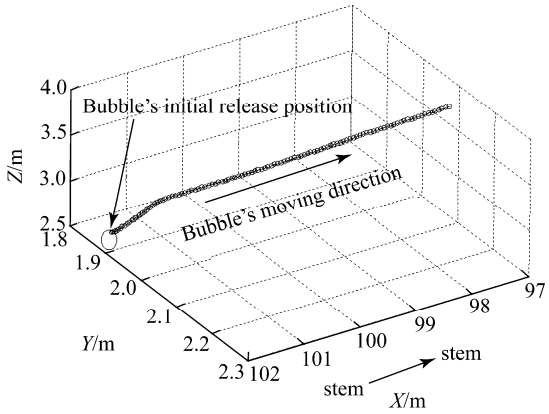

(a) 3-D trajectory of a $0.02D_1$ bubble without vibration

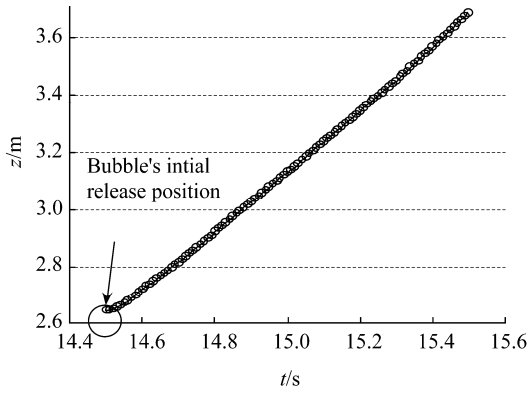

(b) Vertical displacement of a $0.02D_1$ bubble without vibration

Fig.5 Migration of a $0.02D_1$ bubble without vibration

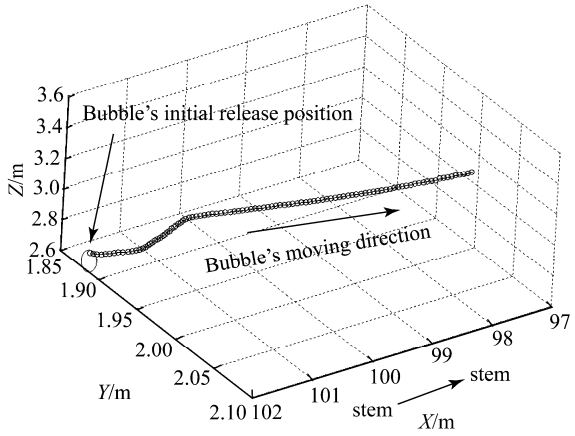

(a) 3-D trajectory of a $0.01D_1$ bubble without vibration

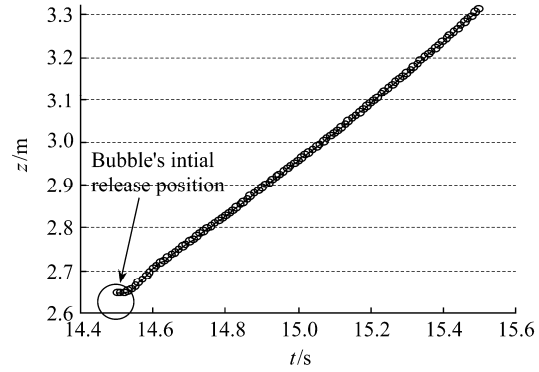

(b) Vertical displacement of a $0.01D_1$ bubble without vibration

Fig.6 Migration of a $0.01D_1$ bubble without vibration

Because of the symmetry of the port and starboard, the port is chosen as the representative to calculate the bubble's trajectory. Fig.5 and Fig.6 are the three-dimensional trajectory and vertical displacement of $0.01D_1$ and $0.02D_1$ bubbles without oscillation, respectively. Because the fourth-order Runge-Kutta method has a strict demand on the time increment, the time step is taken as 0.01 s and the calculation is from 14.5 s to 15.5 s. The initial releasing moment of 14.5 s corresponds to the moment when the vessel heaves to the lowest point in this condition. From Fig.5 and Fig.6, it can be seen that the bubble moves abaft as well as upwards. The trajectory of the bubble is basically smooth except for some turns at an early stage. Comparing Fig.5(b) and Fig.6(b), it's easy to find that a bigger bubble will have a larger upward migration, due to its greater buoyancy.

4.2 With the Influences of Bubble's Oscillation

According to the theoretical analysis above, bubbles will oscillate radially while migrating. The bubble's oscillation will not only affect its drag force, but also add an item $3\dot{R}(\boldsymbol{v}-\boldsymbol{u}_b)/R$, which is actually the momentum change rate generated by added mass change by radial oscillation. In this chapter, Eqs.(2) and (6) are solved simultaneously to get the migration and oscillation of the bubble. $0.02D_1$ and $0.01D_1$ are still taken as the bubbles' initial radii in the calculation.

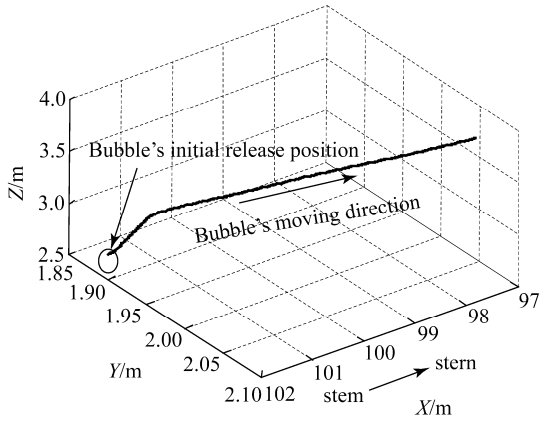

(a) 3-D trajectory of a $0.02D_1$ bubble with vibration

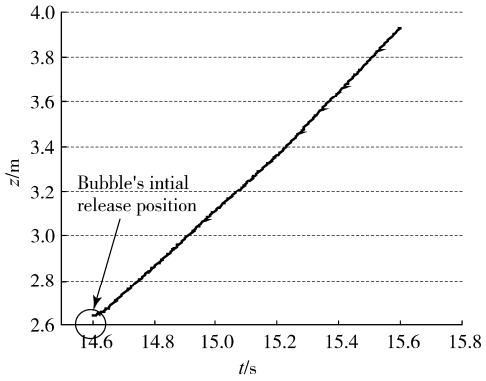

(b) Vertical displacement of a $0.02D_1$ bubble with vibration

Fig.7 Migration of a $0.02D_1$ bubble with vibration

Fig.7 is three-dimensional trajectory and vertical displacement of a $0.02D_1$ bubble with oscillation. When considering the bubble's oscillation, the program becomes more sensitive to time increments. Therefore, the time step is reduced to 0.001 s. The initial releasing moment is 14.6 s, which corresponds to the moment when the vessel heaves to the lowest point in this condition. It can be seen that the moving trend of the bubble is still abaft and upward. In the same computing time, vertical displacement without vibration is 1.05 m; while the one with vibration is 1.29 m, as shown in Fig.5 and Fig.7. It can be seen that a bubble with vibration rises faster than the one without vibration.

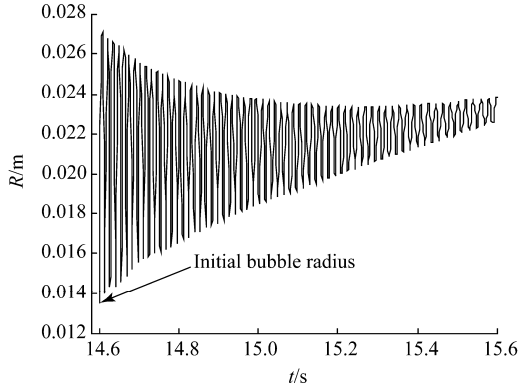

(a) Radius vibration of a $0.02D_1$ bubble

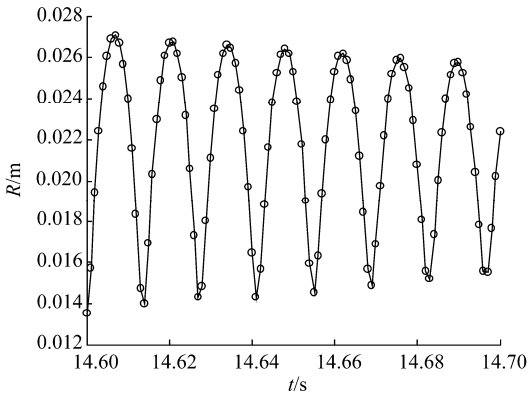

(b) Local magnification of bubble's vibration

Fig.8 Oscillation of a $0.02D_1$ bubble

Fig.8(a) is the curve of oscillation of the bubble radius in the calculation time, and local magnification in the first 0.1 s is shown in Fig.8(b) to express it more clearly. From Fig.8 (a), it is found that the bubble's balance radius increases but the vibration amplitude decreases along with time. This phenomena can be understood because the hydrostatic pressure becomes lower as bubble rises. Additionally, the bubble's radius during the whole vibration process is always bigger than the initial radius of 0.0135 m. Due to larger bubble volume, the buoyancy of the bubble increases, which results in larger rise than the one without vibration. From Fig.8(b), it can be seen that a 0.02 D_1 bubble has a vibration cycle of about 0.013 s and frequency of 75 Hz.

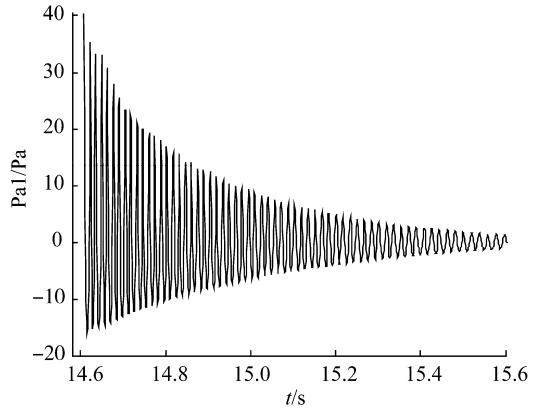

(a) Radiated sound pressure at a measured point

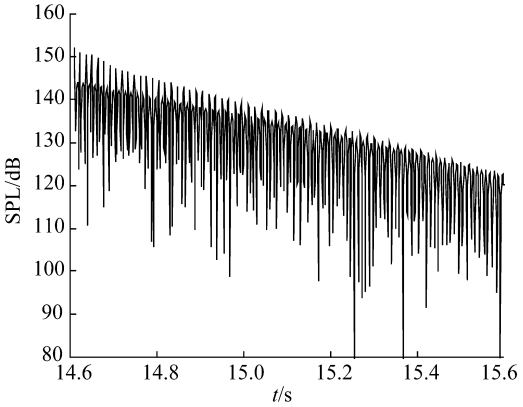

(b) Radiated sound pressure level at a measured point

Fig.9 Radiated sound pressure and SPL of a 0.02D_1 bubble

Fig.9(a) shows radiated sound pressure at a measured point by applying Eq.(8), in which the oscillating bubble equals to a vibration source. The measured point is at a distance of 200 R_0 from the center of the bubble. It is shown in Fig.9 that radiated sound pressure is asymmetrical and attenuates to near zero sharply as it fluctuates around zero. Fig.9(b) shows the variation of the sound pressure level (SPL) by applying Eq.(9). It is found that the SPL decreases along with time. Though the sound pressure level is high, it will not affect the performance of sonar because of its low frequency of 75 Hz.

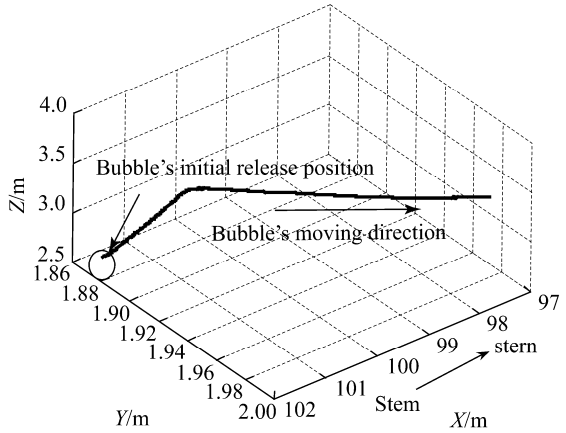

(a) 3-D trajectory of a 0.01D_1 bubble with vibration

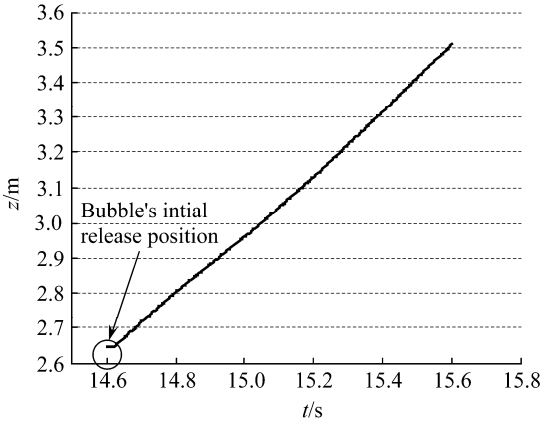

(b) Vertical displacement of a 0.01D_1 bubble with vibration

Fig.10 Migration of a 0.01D_1 bubble with vibration

Fig.10 shows a three-dimensional trajectory and vertical displacement of a 0.01D_1 oscillating bubble. The calculating time and time step remain the same. Contrasting Fig.10 and Fig.6, one can see that oscillation makes the bubble rise faster. In contrasting Fig.10 and Fig.9, one can see that a bubble with smaller oscillation rises slower than the one with larger oscillation.

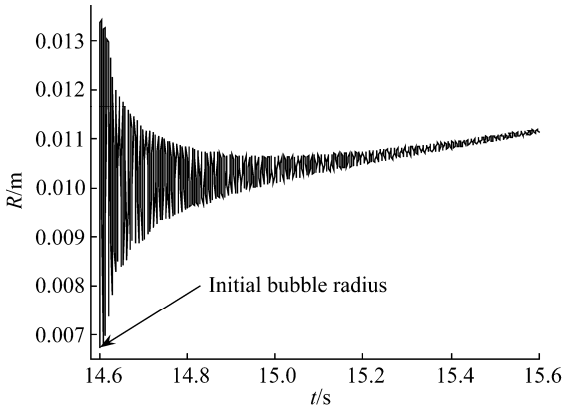

(a) Radius vibration of a 0.01D_1 bubble

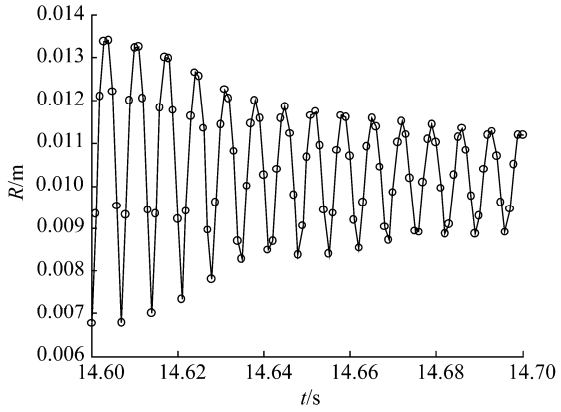

(b) Local magnification of bubble vibration

Fig.11 Oscillation of a 0.01D_1 bubble

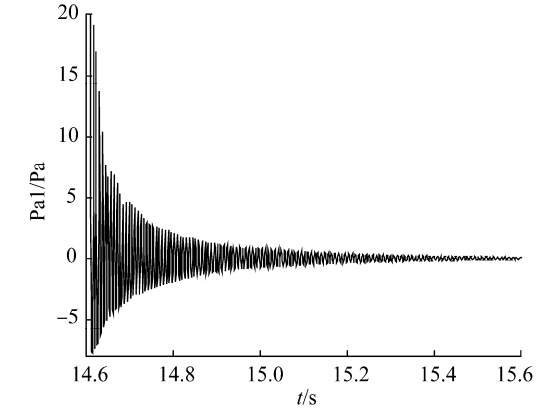

(a) Radiated sound pressure at a measured point

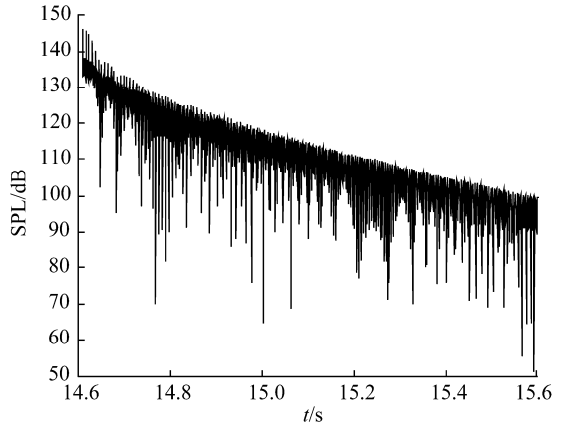

(b) Radiated sound pressure level at a measured point

Fig.12 Radiated sound pressure and SPL of a 0.01D_1 bubble

Fig.11(a) is the radius vibration of a 0.01D_1 bubble, while Fig.11(b) is its local magnification in the first 0.1 s. Contrasting Fig.11 and Fig.8, one can see that the oscillating frequency of a smaller bubble is higher and it has a sharper attenuating trend. From Fig.12(b), it is seen that the oscillating cycle of the 0.01D_1 bubble is about 0.007 s and its frequency is around 143 Hz, which is twice of the 0.02 D_1 bubble. Therefore, the initial radius of the bubble greatly affects the oscillating frequency.

Fig.12 is radiated sound pressure caused by the bubble radial vibration. The measured point is at a distance of 400 R_0 from the center of the bubble. It can be seen that the radiated sound pressure frequency increases and its amplitude decreases faster than that of the 0.02D_1 bubble. Fig.12(b) shows the corresponding SPL. Though the SPL is high, it will not affect the performance of sonar because of its low frequency of 143 Hz.

5 Conclusions

To study the dynamic behavior of a small spherical bubble escaping from the lateral propulsion hole at the stem, this paper suggested the One-way Coupled Particle Tracking Method (OCPTM) to track the bubble. The common commercial Computational Fluid Dynamics software CFX as well as a self-programmed procedure was combined to solve the kinematic and dynamic equations simultaneously. Based on this procedure, the bubble migration, oscillation, and radiated noise were simulated.

Through calculation, the small bubble escaping from the lateral propulsion hole could be seen as an oscillating and translating sphere, which moves abaft and upward. On one hand, the oscillating frequency of the small bubble was relatively low, in the order of hundreds of Hz, which will not affect the performance of sonar. The oscillating frequency became higher as the initial bubble's radius decreased. On the other hand, the bubble with radial oscillation will have a higher rising velocity compared with the one ignoring the effect of oscillation. The radiated sound pressure was asymmetrical and it attenuated to near zero sharply as the bubble rose.

In the next step of the research, the authors would like to consider the motion of masses of air with the length scale in the order of half the diameter of the lateral propulsion hole, as well as their influence on the ambient flow around the lateral propulsion hole.

References

Cole RH (1948). *Underwater Explosion.* Princeton University Press, New Jersey, 118-127.

Fitzpatrick N, Strasberg M (1958). *Hydrodynamic sources of sound, 2nd Symposium on Naval Hydrodynamics*, National Academy Press, Washington D.C., 201-205.

Fu HP, Wan PC (2011). Numerical simulation on ship bubbly wake. *Journal of Marine Science and Application*, **10**(4), 411-418.

Gilmore FR (1952). The growth and collapse of a spherical bubble in a viscous compressible liquid. Hydrodynamic Lab California Institute, United States, Technical Report. No. **26**(4), 117-125.

Gu JN，Zhang ZH，Zhang XH (2007). Numerical simulation of bubble distribution characters in ship's far field wakes, *Acta Photonica Sinica*，**36**(8), 1504-1509 (in Chinese).

Haberman WL, Morton RK (1953). An experimental investigation of the drag and shape of air bubbles rising in various liquids.

DTMB Report. No. 802.

Hsiao CT, Chahine GL (2003). Scaling effect on prediction of cavitation inception in a line vortex flow. *Journal of Fluid Engineering*, **125**, 53-60.

Hsiao CT, Chahine GL, Liu HL (2000). Scaling effect on bubble dynamics in a tip vortex flow: prediction of cavitation inception and noise. Dynaflow Incorporation, Jessup, United States. Technical Report No. 98007-NSWC.

Plesset MS, Chapman RB (1971). Collapse of an initially spherical vapor cavity in the neighborhood of a solid boundary. *Journal of Fluid Mechanics*, **47**, 283-290.

Prosperetti A(2002).Bubbles. *Physics of Fluids*, **16** (6),1852-1865.

Rayleigh JW (1917). On the pressure developed in a liquid during the collapse of a spherical cavity. *Philosophy Magazine*, **34**, 94-98.

Shi SW, Jiang XZ, Shi M, Wang JA (2007). Movement characteristic of bubbles in ship wakes. *Journal of Wuhan University of Technology (Transportation Science & Engineering)*, **31**(5), 764-769. (in Chinese)

Vries AWG, Biesheuvel A, Wijngaarden LV(2002). Notes on the path and wake of a gas bubble rising in pure water. *International Journal of Multiphase Flow*, **28**, 1823-1835.

Wang ZY, Tong AY (2008). Deformation and oscillations of a single gas bubble rising in a narrow vertical tube. *International Journal of Thermal Sciences*, **47**, 221-228.

Appendix

Derivation of the Modified Rayleigh-Plesset Euation:

The total velocity of any point in the field $\boldsymbol{u}_{total}$ can be expressed via the Helmholtz decomposition as the sum of bubble induced velocity $\boldsymbol{u}$ and the flow field velocity $\boldsymbol{v}$.

$$\boldsymbol{u}_{total} = \boldsymbol{u} + \boldsymbol{v} = \nabla\varphi + \boldsymbol{v} \tag{A1}$$

where the velocity induced by the bubble presence is assumed to be expressed as $\boldsymbol{u} = \nabla\varphi$. Based on the assumption in the text, the flow field $\boldsymbol{v}$ is assumed to remain unaffected by the bubble presence and dynamics.

Substituting the the decomposited total velocity $\boldsymbol{u}_{\text{total}}$ into the NS equation, one will get:

$$\begin{aligned}&\frac{\partial}{\partial t}(\boldsymbol{u}+\nu)-(\boldsymbol{u}+\boldsymbol{v})\times[\nabla\times(\boldsymbol{u}+\boldsymbol{v})]+\frac{1}{2}\nabla|\boldsymbol{u}+\boldsymbol{v}|^2 = \\ &\boldsymbol{g}-\frac{\nabla P}{\rho}=\nu\nabla^2(\boldsymbol{u}+\boldsymbol{v})\end{aligned} \tag{A2}$$

where the pressure P is the sum of bubble induced pressure and ambient pressure P_v. With the assumption that the undisturbed ambient flow satisfies the NS equation, one has,

$$\frac{\partial \boldsymbol{v}}{\partial t} - \boldsymbol{v}\times(\nabla\times\boldsymbol{v}) + \frac{1}{2}\nabla|\boldsymbol{v}|^2 = \boldsymbol{g} - \frac{\nabla P_v}{\rho} + \nu\nabla^2\boldsymbol{v} \tag{A3}$$

Substitute Eq.(A.3) into Eq.(A.2), one will get

$$\nabla\left[\frac{\partial\varphi}{\partial t}+\frac{1}{2}|\nabla\varphi|^2+\boldsymbol{v}\cdot\nabla\varphi+\frac{P-P_v}{\rho}\right]=\nabla\varphi\times(\nabla\times\boldsymbol{v}) \tag{A4}$$

In not producing d$\boldsymbol{l}$ to the both hands of Eq.(A4), one has,

$$\mathrm{d}\left[\frac{\partial\varphi}{\partial t}+\frac{1}{2}|\nabla\varphi|^2+\boldsymbol{v}\cdot\nabla\varphi+\frac{P-P_v}{\rho}\right]=\nabla\varphi\times(\nabla\times\boldsymbol{v})\cdot\mathrm{d}\boldsymbol{l} \tag{A5}$$

Integrating Eq.(A5) along the vortex line, the right hand of (A5) becomes zero,

$$\nabla\varphi\times(\nabla\times\boldsymbol{v})\cdot\mathrm{d}\boldsymbol{l}=\left[(\nabla\times\boldsymbol{v})\cdot\mathrm{d}\boldsymbol{l}\right]\cdot\nabla\varphi=0 \tag{A6}$$

Since $\varphi = 0$ at infinite, the following is obtained:

$$\frac{\partial\varphi}{\partial t}+\frac{1}{2}|\nabla\varphi|^2+\boldsymbol{v}\cdot\nabla\varphi+\frac{P-P_v}{\rho}=\frac{P(\infty)-P_v(\infty)}{\rho}=0 \tag{A7}$$

Eq.(A7) is an integral in the absolute reference frame, where the velocity potential is $\varphi(\boldsymbol{x},t)$, and it is not necessary to find the expression in the moving reference frame, where the velocity potential is $\varphi'(\boldsymbol{x}',t)$. Velocity potential is the same both in the absolute reference frame and in the moving reference frame:

$$\varphi(\boldsymbol{x},t)=\varphi'(\boldsymbol{x}'(\boldsymbol{x},t),t) \tag{A8}$$

Applying the chain derivation to Eq.(A8),

$$\left(\frac{\partial\varphi}{\partial t}\right)_x=\nabla'\varphi'\cdot\left(\frac{\partial\boldsymbol{x}'}{\partial t}\right)_x+\left(\frac{\partial'\varphi'}{\partial t}\right)_{x'} \tag{A9}$$

where $\nabla'\varphi' = \boldsymbol{u}$ and $\left(\frac{\partial\boldsymbol{x}'}{\partial t}\right)_x = -\boldsymbol{V}_e$ is the transport velocity of the moving reference frame.

Substituting Eq.(A9) into Eq.(A7), one has

$$\frac{\partial'\varphi'}{\partial t}-\boldsymbol{V}_e\cdot\boldsymbol{u}+\frac{1}{2}\boldsymbol{u}^2+\boldsymbol{u}\cdot\boldsymbol{v}=\frac{P_v-P}{\rho} \tag{A10}$$

The velocity potential induced by an oscillating and moving the spherical bubble can be decomposited into two parts: one is a source, and the other is a dipole. So the absolute velocity potential in the moving reference frame is expressed as:

$$\varphi'=-\frac{\dot{R}R^2}{r}+V(t)\cos\theta\left(\frac{R^3}{2r^2}\right) \tag{A11}$$

where $V(t)=\boldsymbol{v}-\boldsymbol{u}_b$ is the relative slip velocity of between the carrying liquid and the bubble center. Here it is assumed that the bubble is small so that the ambient flow can be treated as a uniform flow around the bubble locally.

Substituting Eq.(A11) into Eq.(A10),

$$-\ddot{R}R-2\dot{R}^2+\frac{\partial V}{\partial t}\frac{R}{2}\cos\theta+\frac{3}{2}\dot{R}V\cos\theta+V\dot{R}\cos\theta-$$
$$V^2\cos^2\theta+\frac{1}{2}V^2\sin^2\theta+\frac{1}{2}\dot{R}^2-V\dot{R}\cos\theta+\frac{1}{2}V^2\cos^2\theta+$$
$$\frac{1}{8}V^2\sin^2\theta+u_xv_x+u_yv_y+u_zv_z=\frac{P_v-P_R}{\rho} \tag{A12a}$$

where

$$u_x=(\frac{\partial\varphi}{\partial r}\sin\theta+\frac{\partial\varphi}{r\partial\theta}\cos\theta)\cos\eta,$$
$$u_y=(\frac{\partial\varphi}{\partial r}\sin\theta+\frac{\partial\varphi}{r\partial\theta}\cos\theta)\sin\varphi,$$
$$u_z=\frac{\partial\varphi}{\partial r}\cos\theta-\frac{\partial\varphi}{r\partial\theta}\sin\theta.$$

Simplifying equation (A12a),

$$-\ddot{R}R-\frac{3}{2}\dot{R}^2+(\frac{\partial V}{\partial t}\frac{R}{2}+\frac{3}{2}\dot{R}V)\cos\theta-\frac{1}{2}V^2+$$
$$\frac{9}{8}V^2\sin^2\theta+u_xv_x+u_yv_y+u_zv_z=\frac{P_v-P_R}{\rho} \tag{A12b}$$

In this paper, the concern is the average pressure on the spherical bubble, not the pressure on one single node, so an average equation is obtained by integrating over the bubble surface with θ and η:

$$\frac{1}{4\pi R^2}\int_0^{2\pi}\mathrm{d}\varphi\int_0^{\pi}(\frac{\partial V}{\partial t}\frac{R}{2}+\frac{3}{2}\dot{R}V)\cos\theta\cdot R^2\cdot\sin\theta\mathrm{d}\theta=0 \tag{A13a}$$

$$\frac{1}{4\pi R^2}\int_0^{2\pi}\mathrm{d}\varphi\int_0^{\pi}\frac{9}{8}V^2\sin^2\theta\cdot R^2\cdot\sin\theta\mathrm{d}\theta=\frac{3}{4}V^2 \tag{A13b}$$

$$\frac{1}{4\pi R^2}\int_0^{2\pi}\int_0^{\pi}v_x\left[(u_r\sin\theta+u_\theta\cos\theta)\cos\varphi\right]\cdot R^2\sin\theta\mathrm{d}\theta\mathrm{d}\varphi=0 \tag{A13c}$$

$$\frac{1}{4\pi R^2}\int_0^{2\pi}\int_0^{\pi}v_y\left[(u_r\sin\theta+u_\theta\cos\theta)\cos\varphi\right]\cdot R^2\sin\theta\mathrm{d}\theta\mathrm{d}\varphi=0 \tag{A13d}$$

$$\frac{1}{4\pi R^2}\int_0^{2\pi}\mathrm{d}\varphi\int_0^{\pi}v_z(u_r\cos\theta-u_\theta\sin\theta)\cdot R^2\sin\theta\mathrm{d}\theta=$$
$$\frac{v_z}{2}\int_0^{\pi}(\dot{R}\cos\theta\sin\theta-V(t)\cos^2\theta\sin\theta+\frac{1}{2}V(t)\sin^3\theta)\mathrm{d}\theta=$$
$$\frac{v_z}{2}(0-\frac{2}{3}V(t)+\frac{2}{3}V(t))=0 \tag{A13e}$$

Substituting Eq.(A8) into Eq.(A7b), one will get the Modified Rayleigh-Plesset Equation considering the effect of the relative slip velocity between the bubble and the carrying liquid:

$$-\ddot{R}R-\frac{3}{2}\dot{R}^2+\frac{1}{4}V^2=\frac{P_v-P_R}{\rho} \tag{A14}$$

It is assumed that the bubble contains non-condensable gas and liquid vapor. The non-condensable gas is assumed to satisfy a polytropic law with an exponent γ, and the surface tension and viscosity are considered here, so the pressure outside the bubble is:

$$P_R=P_c+P_{g0}(\frac{R_0}{R})^{3\gamma}-\frac{2\sigma}{R}-4\mu\frac{\dot{R}}{R} \tag{A15}$$

Substituting Eq.(A10) into Eq.(A9), one will get Eq.(2) as follow.

$$R\ddot{R}+\frac{3}{2}\dot{R}^2=\frac{1}{\rho}\left[P_c+P_{g0}(\frac{R_0}{R})^{3\gamma}-\frac{2\sigma}{R}-4\mu\frac{\dot{R}}{R}-P_v\right]+\frac{(\boldsymbol{v}-\boldsymbol{u_b})^2}{4} \tag{A16}$$

Baoyu Ni was born in 1986. He is a PhD candidate at Harbin Engineering University, and a visiting research student at University College London (UCL). His current research interests are underwater bubble dynamics, and coupled fluid-structure analysis.

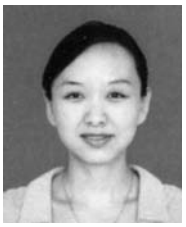

Shaoshi Dai was born in 1976. She is a lecturer at College of Shipbuilding Engineering, Harbin Engineering University. Her current research interests include fluid-structure interaction, structural dynamics, *etc*.

Rui Han was born in 1989. She is a graduate at Harbin Engineering University, and her current research interest is bubbly flow.

Longquan Sun was born in 1983. He is a lecturer at College of Shipbuilding Engineering, Harbin Engineering University. His current research interests are ship structural dynamics and underwater acoustic design.

Hailong Chen was born in 1980.He is a research fellow at Harbin Engineering University. His current research interests include fluid-structure interaction, structural dynamics, *etc*.